NACA RM A55C28

NACA

RESEARCH MEMORANDUM

EXPLORATORY INVESTIGATION OF THE LOW-SPEED STATIC STABILITY OF A CONFIGURATION EMPLOYING THREE IDENTICAL TRIANGULAR WING PANELS AND A BODY OF EQUAL LENGTH

By Noel K. Delany

Ames Aeronautical Laboratory
Moffett Field, Calif.

NATIONAL ADVISORY COMMITTEE
FOR AERONAUTICS

WASHINGTON

April 29, 1955
Declassified May 8, 1958

NATIONAL ADVISORY COMMITTEE FOR AERONAUTICS

RESEARCH MEMORANDUM

EXPLORATORY INVESTIGATION OF THE LOW-SPEED STATIC STABILITY OF A CONFIGURATION EMPLOYING THREE IDENTICAL TRIANGULAR WING PANELS AND A BODY OF EQUAL LENGTH

By Noel K. Delany

SUMMARY

An experimental investigation has been conducted at low speeds of the static-stability characteristics of a simplified model of an unusual configuration. The model had three identical triangular airfoils of low aspect ratio. One of the airfoils was mounted vertically on top of a body of revolution as a fin and the other two were mounted as the main lifting surfaces. The leading edges of the airfoils were swept back 73.9°. The body had the same length as the airfoils.

Results of tests of the simplified model of the configuration are presented for a large range of angles of attack and sideslip. Results of a cursory investigation of elevator and rudder effectiveness and of the effects of changes in dihedral are also included.

With the three airfoils spaced 120° apart (wing dihedral angle -30°) the changes of the static-stability parameters with angle of attack and angle of sideslip were gradual for angles of attack and angles of sideslip up to about 20°. The moment center for neutral static longitudinal stability was about 0.41 of the mean aerodynamic chord behind the leading edge of the mean aerodynamic chord.

INTRODUCTION

A possible airplane configuration having three identical triangular airfoils of low aspect ratio radiating symmetrically from a central body that does not protrude ahead of the wings has been suggested as a promising arrangement for flight at very high speeds. If such an arrangement were to make conventional landings it would appear that a minimum of

landing-gear weight would be entailed with one of the airfoils vertical on top of the body and the other two as a wing having negative dihedral. With the airfoils symmetrically disposed about the body, the angular spacing would be 120° and the wing would have a dihedral angle of -30°.

Since relatively little is known about the approach, landing, and take-off characteristics of such an arrangement, an investigation of the static stability of a simplified model at low speed was undertaken. Measurements of the forces and moments were made for a large range of angles of attack and sideslip for the basic configuration. The effectiveness of flap-type controls and the effects of changes in dihedral were also measured. The investigation was conducted in a 7- by 10-foot wind tunnel at the Ames Aeronautical Laboratory at a Mach number of about 0.25 which corresponded to a Reynolds number of about 4.5 million based on the mean aerodynamic chord.

NOTATION

A diagram showing the system of axes and the positive directions of forces and moments used in presenting the data is shown in figure 1. The axes of all forces and moments pass through the moment center of the model. Both the body axes and the stability system of axes are defined in figure 1; however, unless otherwise specified the results presented are with respect to the body axes. The symbols used in this report are defined as follows:

b wing span (twice the panel span), ft

$\bar{c}$ mean aerodynamic chord of the wing, $\dfrac{\int_0^{b/2} c^2 dy}{\int_0^{b/2} c\, dy}$, ft

c wing chord parallel to plane of symmetry, ft

C_A axial-force coefficient, $\dfrac{F_A}{qS}$

C_{D_S} drag coefficient referred to stability axes, $\dfrac{F_{D_S}}{qSb}$

C_L lift coefficient, $\dfrac{F_L}{qS}$

C_l rolling-moment coefficient referred to body axes, $\dfrac{M_X}{qSb}$

C_{l_s} rolling-moment coefficient referred to stability axes, $\frac{M_{X_s}}{qSb}$

C_m pitching-moment coefficient, $\frac{M_Y}{qS\bar{c}}$

C_N normal-force coefficient, $\frac{F_N}{qS}$

C_n yawing-moment coefficient referred to body axes, $\frac{M_Z}{qSb}$

C_{n_s} yawing-moment coefficient referred to stability axes, $\frac{M_{Z_s}}{qSb}$

C_Y side-force coefficient, $\frac{F_Y}{qS}$

F_A axial force, positive along -X axis, lb

F_{D_s} drag force, positive along $-X_s$ axis, lb

F_L lift force, positive along $-Z_s$ axis, lb

F_N normal force, positive along -Z axis, lb

F_Y side force, positive along the Y or Y_s axis, lb

$\frac{L}{D}$ ratio of lift to drag

M_X rolling moment about the X axis, positive clockwise looking forward, ft-lb

M_{X_s} rolling moment about the X_s axis, positive clockwise looking forward, ft-lb

M_Y pitching moment about the Y or Y_s axis, positive moment raises the nose, ft-lb

M_Z yawing moment about Z axis, positive moment rotates nose to right, ft-lb

M_{Z_s} yawing moment about Z_s axis, positive moment rotates nose to right, ft-lb

q dynamic pressure, lb/sq ft

S wing area (twice panel area), sq ft

V_o free-stream velocity, ft/sec

V_s sinking speed, ft/sec

W weight of assumed airplane, lb

α angle of attack, deg

β angle of sideslip, deg

Γ dihedral angle, deg

δ_r rudder deflection, deg

δ_e elevator deflection, deg

X longitudinal body axis, in vertical plane of symmetry and coincident with center line of body, positive forward

X_s longitudinal stability axis, parallel to the projection of the relative wind on the vertical plane of symmetry, positive forward

Y lateral body axis, perpendicular to vertical plane of symmetry, positive to right when looking forward

Y_s lateral-stability axis, perpendicular to vertical plane of symmetry, positive to right when looking forward

Z vertical body axis, in vertical plane of symmetry and perpendicular to the longitudinal and lateral body axes, positive downward.

Z_s vertical stability axis, in vertical plane of symmetry and perpendicular to the relative wind, positive downward

MODEL AND APPARATUS

The model consisted of three triangular airfoils symmetrically arranged around a circular cylinder with an ogival nose as shown in figure 2. The wing surfaces were 3/4-inch Douglas fir plywood with blunt trailing edges and sharpened leading edges of solid mahogany. The wood was finished with a surface sealer, but a high degree of smoothness was not attempted. The panels were attached to the body with sheet-metal brackets inlaid flush into the airfoils but external to the cylindrical

surface of the body so as to facilitate changing the angular relation of the wings. A photograph of the model in the wind tunnel is shown in figure 3.

The model was supported on a sting-mounted, four-component, strain-gage balance contained within the body. The diameter of the sting at the base of the body was 3.1 inches. A static-pressure orifice was installed in the annular space between the sting and the body to permit measurement of the base pressure.

Deflected rudder and elevators were simulated by full-span (at the hinge line) split flaps made of sheet metal and attached to the appropriate surfaces with wedge-shaped brackets. The chords of the flaps were 6 percent of the root chord of the wings. The tips of the flaps were cut off square. A photograph of the model with one of the flaps deflected 16° is shown in figure 4.

The pertinent geometric characteristics of the wing panels are tabulated below:

Aspect ratio of panel	0.58
Root chord, ft	3.96
Span, body center line to tip, ft	1.14
Area, sq ft	2.26
Mean aerodynamic chord, ft	2.64
Sweepback of leading edge, deg	73.9

TESTS AND REDUCTION OF DATA

The model support permitted only a rotation of the model about a vertical axis passing through the moment center; hence, the angle of attack and angle of sideslip could not be varied independently. With one of the airfoils horizontal (considered the vertical fin), the angle of attack was varied at 0° sideslip, and with the same airfoil vertical, the angle of sideslip was varied at 0° angle of attack. Intermediate settings of the angle of bank produced attitudes of the model which combined finite angles of attack and sideslip. Data for specific angles of attack combined with sideslip were obtained by cross-plotting the basic wind-tunnel data for the model set to various intermediate angles of bank.

All forces and moments were measured relative to a system of orthogonal axes that were fixed with respect to the model (body axes). Figure 1 defines the angles, forces, and moments relative to both the body axes and the stability axes. Unless otherwise specified, the data

presented are referred to the body axes. The moment center, about which the data are presented, was 0.37 of the mean aerodynamic chord behind the leading edge of the mean aerodynamic chord. For a given attitude of the model in the wind tunnel, and with the four-component strain-gage balance properly alined relative to the model F_N, F_A, M_Y, and M_X were measured. For the same attitude of the model in the wind tunnel but with the balance rotated 90° about its longitudinal axis from the above position, F_Y, F_A, M_Z, and M_X were measured. Hence, for conditions where three force and three moment components were desired, it was necessary to obtain data for both positions of the balance relative to the model.

The average pressure at the base of the model was measured, and data presented have been corrected to correspond to a base pressure equal to free-stream static pressure. Because of the uncertainty of tunnel constriction effects and the exploratory nature of the investigation, no tunnel-wall corrections have been applied to the results.

RESULTS AND DISCUSSION

Several construction features were used in the model for simplicity which probably would not be incorporated in an airplane. Some of these features, such as the airfoil section and the wing-body juncture may have affected the aerodynamic characteristics of the model; but the results are considered sufficiently accurate for a preliminary evaluation of some low-speed characteristics of the configuration.

The lift coefficient, pitching-moment coefficient, and lift-drag ratio of the model with -30° of dihedral and with the elevators deflected 0°, -8°, and -16° are shown in figure 5 for a large angle-of-attack range. It is noted that an elevator deflection of -16° balanced the model at an angle of attack of 20° and a lift coefficient of 0.64. The variation of pitching-moment coefficient with lift coefficient was relatively linear up to an angle of attack of about 24° (balanced C_L approximately 0.75). The slopes of the pitching-moment curves indicate the moment center for neutral stability to have been about 0.41 of the mean aerodynamic chord behind the leading-edge of the mean aerodynamic chord or 0.61 of the root chord behind the leading edge of the root chord.

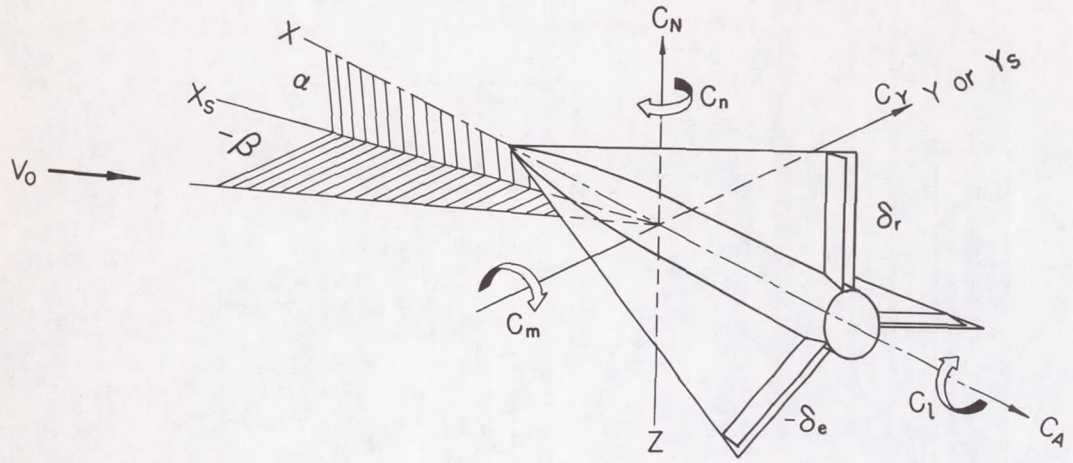
Shown with the lift-drag ratios in figure 5 are lines of constant sinking speed calculated for a wing loading of 20 pounds per square foot and sea-level conditions. It appears that the sinking speed without thrust would be much higher than is currently considered acceptable. A reduction of wing loading to 15 pounds per square foot reduces the estimated sinking speed for a C_L of 0.5 from 58 feet per second, as shown in figure 5, to 48 feet per second. The corresponding flight speeds for these two conditions would be 105 knots and 87 knots, respectively.

The variation with angle of sideslip of yawing-moment, rolling-moment, and side-force coefficients with reference to the body axes for the model with a dihedral of -30° is presented in figures 6(a), (b), and (c) for several angles of attack. The corresponding normal-force, pitching-moment, and axial-force coefficients are presented in figures 6(d), (e), and (f). The changes of these coefficients with angle of sideslip were relatively linear for angles of attack and sideslip up to about 20°. The effects of angle of attack on the static-stability parameters C_{n_β} and C_{l_β}, which were derived from the data in figure 6 for a small range of sideslip angles near zero, are presented in figure 7. Also shown is the variation with angle of attack of these parameters referred to the stability system of axes (normally used for stability computations). There was a small negative-dihedral effect (C_{l_β} with reference to the stability axes was positive) for angles of attack up to about 22°, and the static directional-stability parameter C_{n_β} at an angle of attack of 24° decreased to about half of that at an angle of attack of 0°.

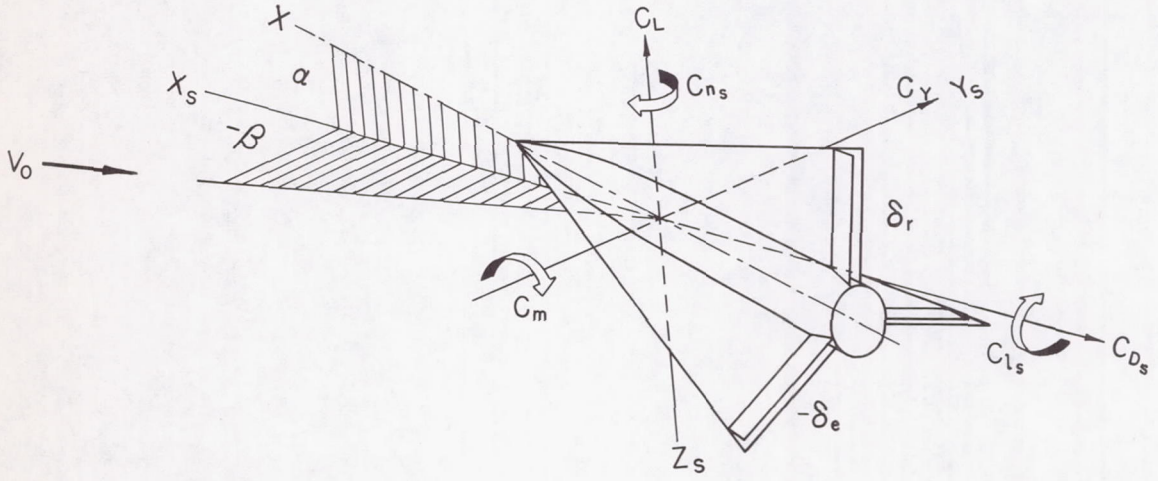
The effect of rudder deflection on the yawing-moment, rolling-moment, and side-force coefficients (with reference to the body axes) for the model with -30° dihedral and an angle of attack of 0° is shown in figure 8. It is noted that for 16° of left-rudder deflection, the model balanced at a sideslip angle of 14°. The effect of angle of attack on the rudder effectiveness was not measured; however, it might be expected that the rudder effectiveness $C_{n_{\delta_r}}$ would vary similarly to C_{n_β} with changes of angle of attack. Under this assumption it appears that the variation of C_n with β would be positive for a rudder deflection of 16° up to angles of attack and angles of sideslip of at least 20°.

The effects of changes of dihedral on the force and moment components (with reference to the body axes) in sideslip for an angle of attack of 0° are presented in figure 9. The effects of dihedral angle on the static-stability parameters C_{n_β} and C_{l_β}, which were derived from the data in figure 9 for a small range of sideslip near zero, are summarized in figure 10.

Ames Aeronautical Laboratory
National Advisory Committee for Aeronautics
Moffett Field, Calif., Mar. 28, 1955



(a) Body axes.



(b) Stability axes.

Figure 1.- Systems of axes and sign convention.

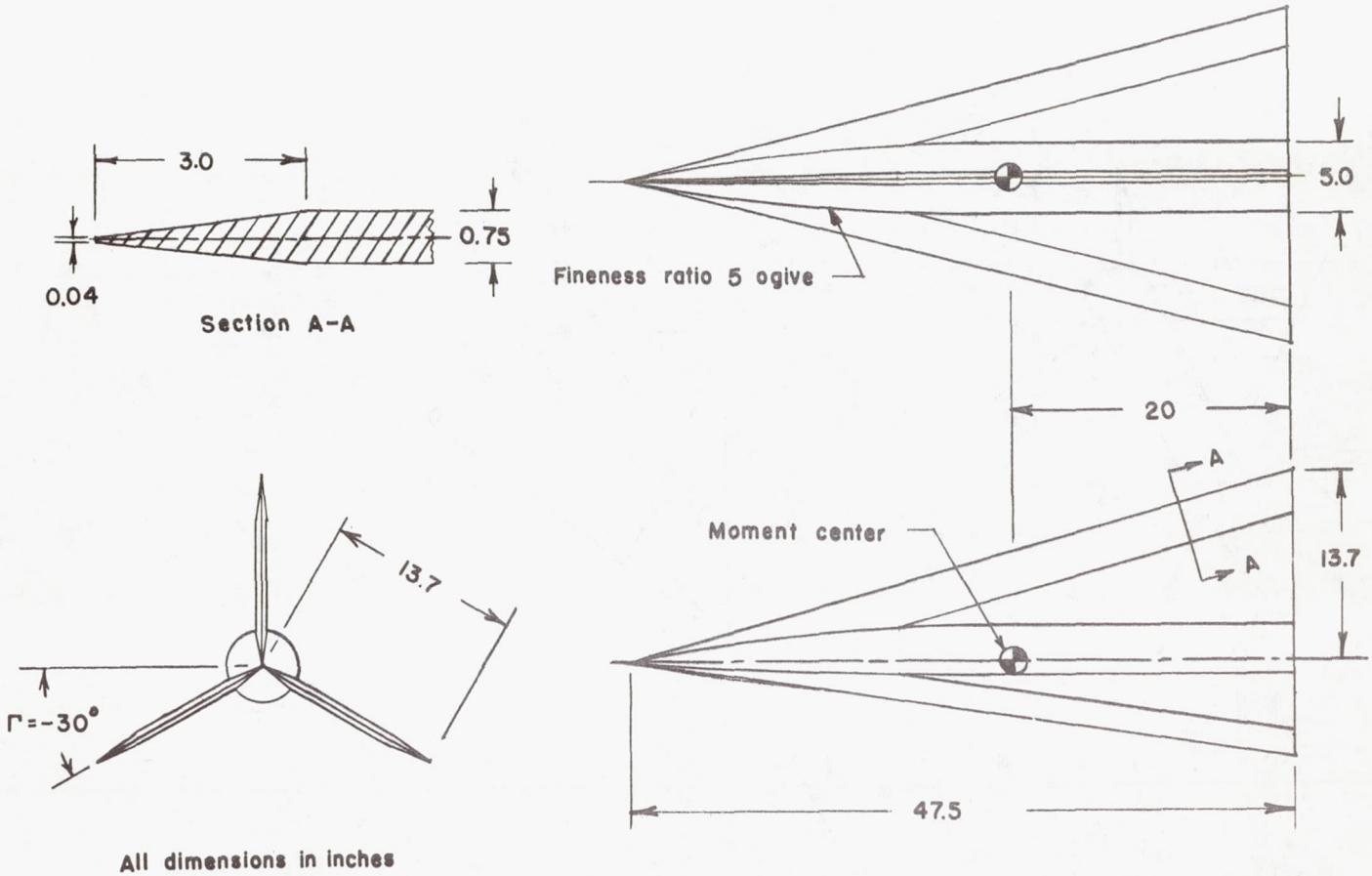
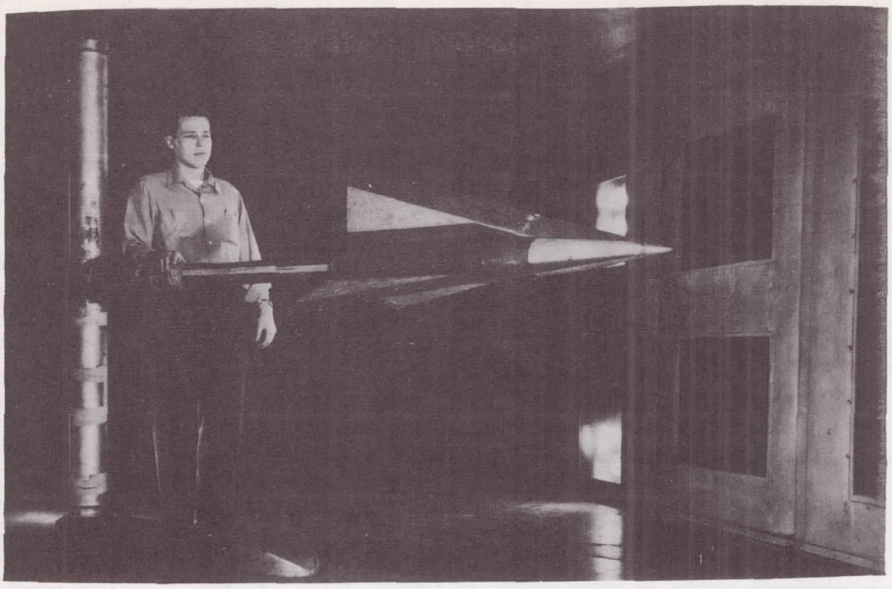
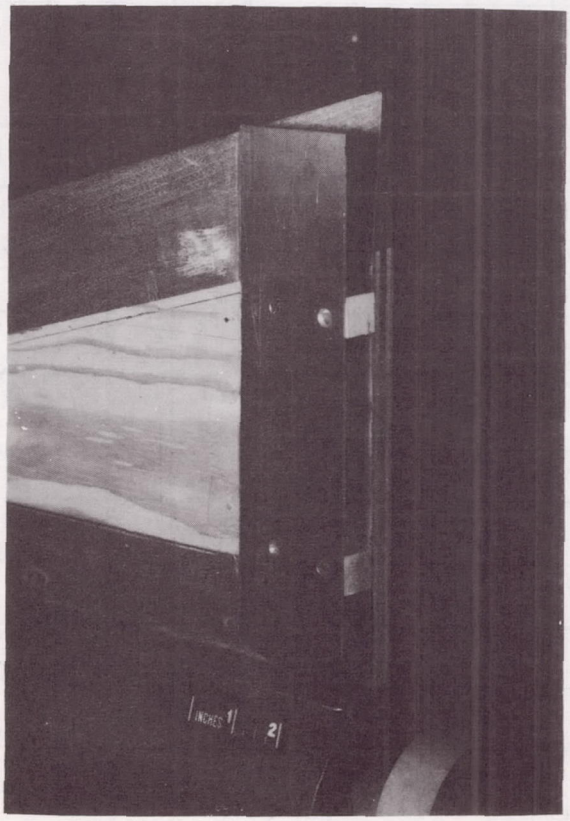


Figure 2.- Sketch of model.



A-20207

Figure 3.- Photograph of the model in the wind tunnel.



A-20206

Figure 4.- Photograph of one of the controls on the model deflected 16°.

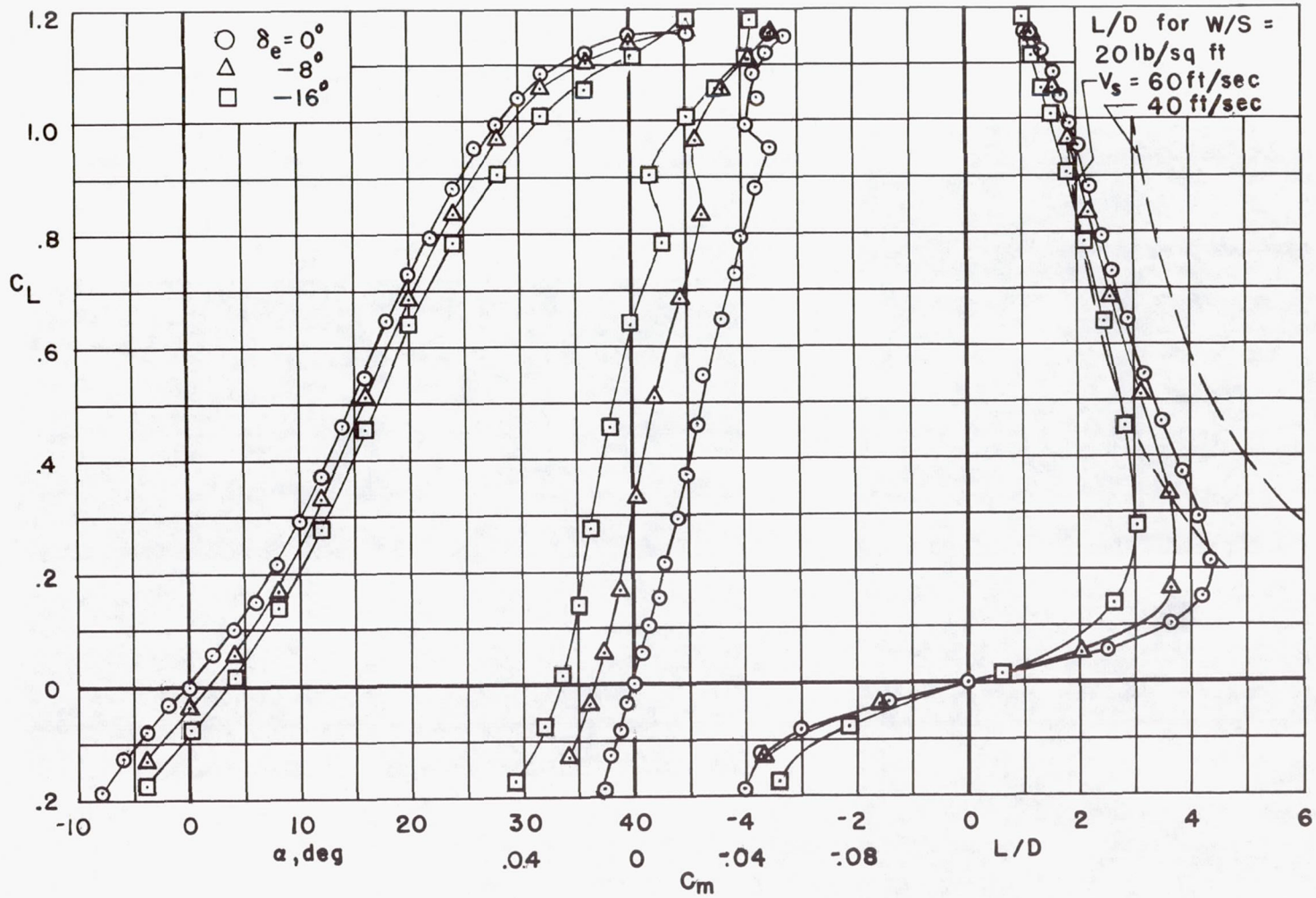
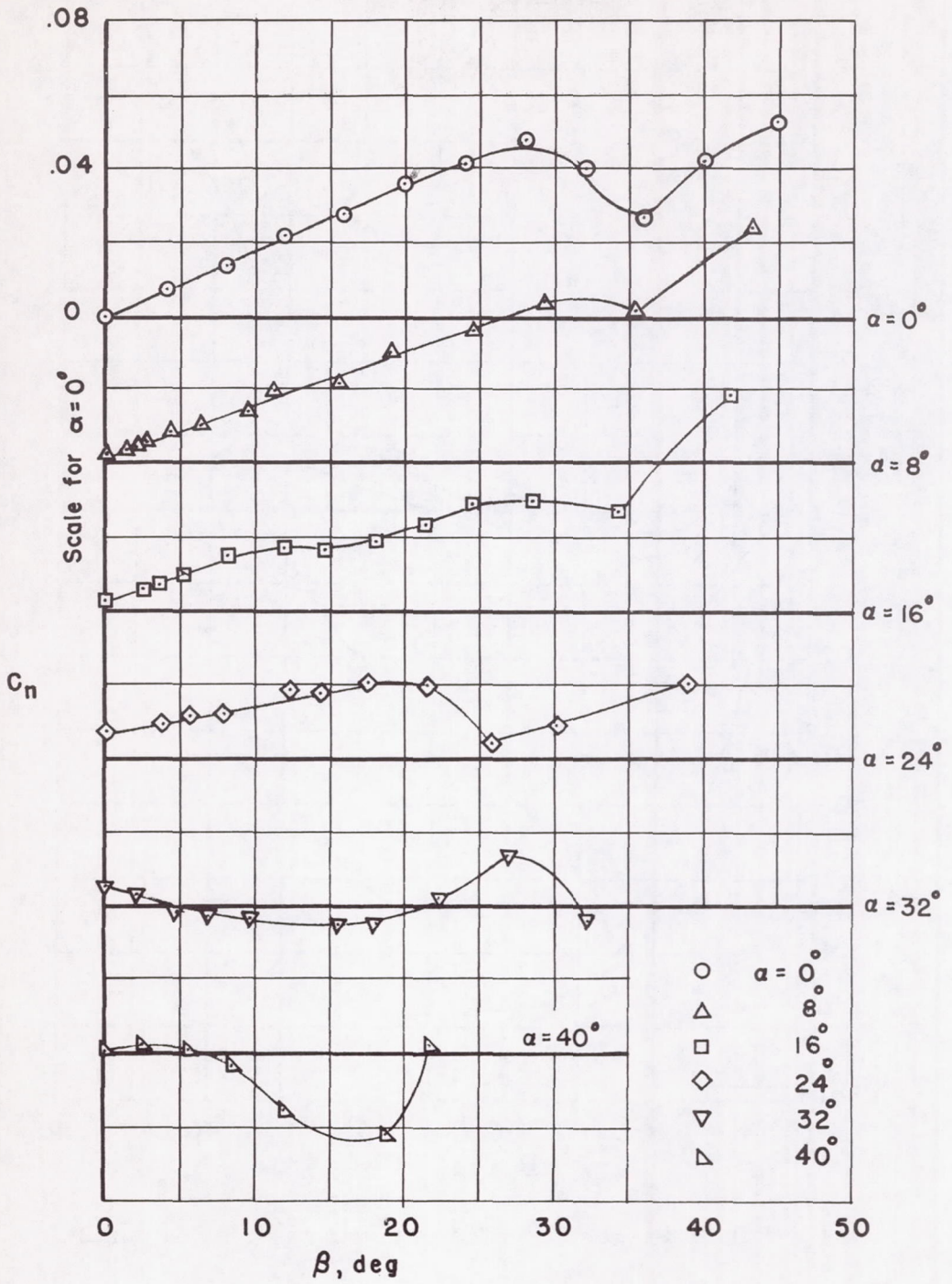
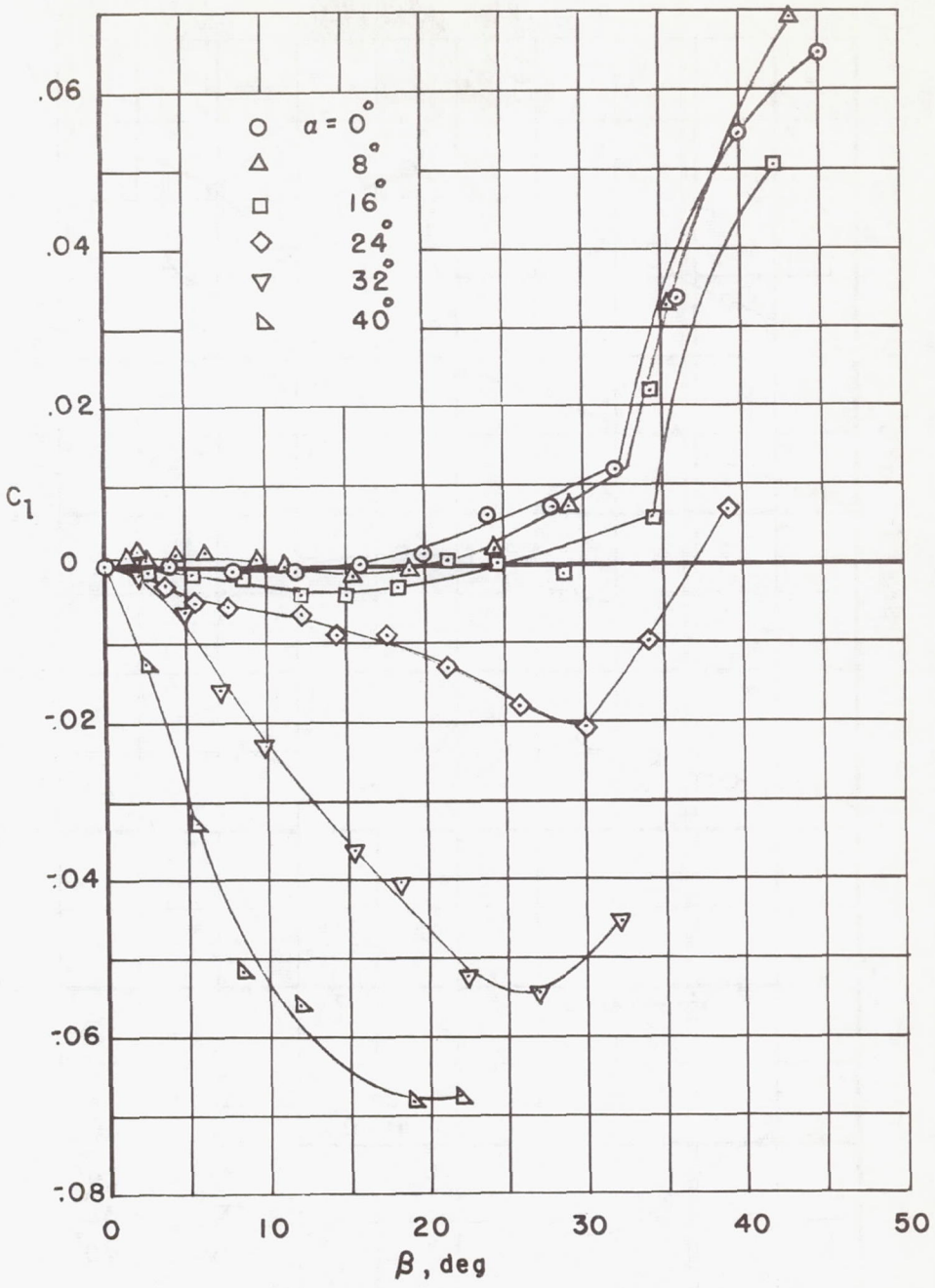


Figure 5.- Static longitudinal-stability characteristics for several elevator deflections; $\Gamma = -30^{\circ}$.



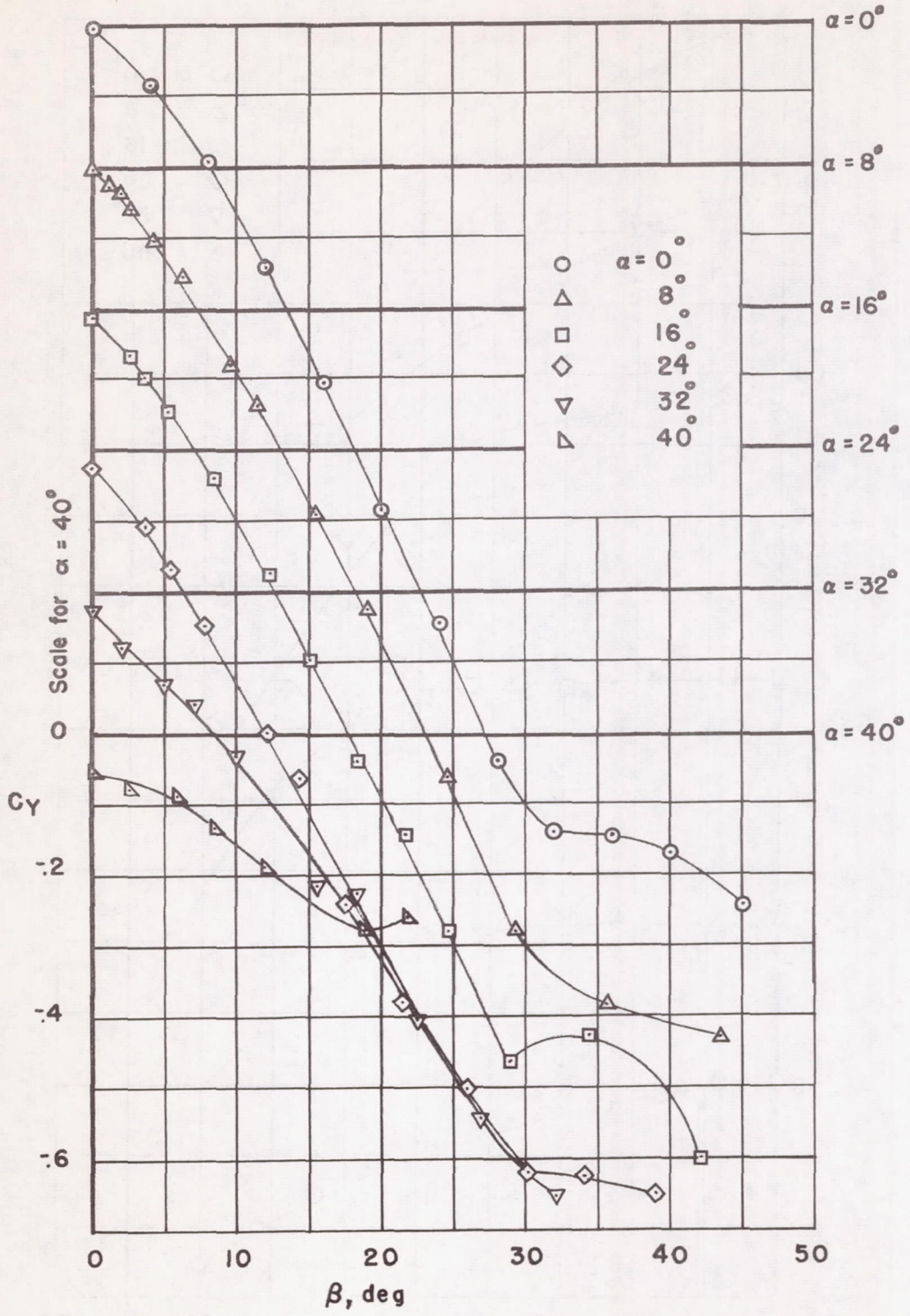
(a) Yawing-moment coefficient versus sideslip angle.

Figure 6.- Force and moment coefficients in sideslip for several angles of attack; $\Gamma = -30^{\circ}$.



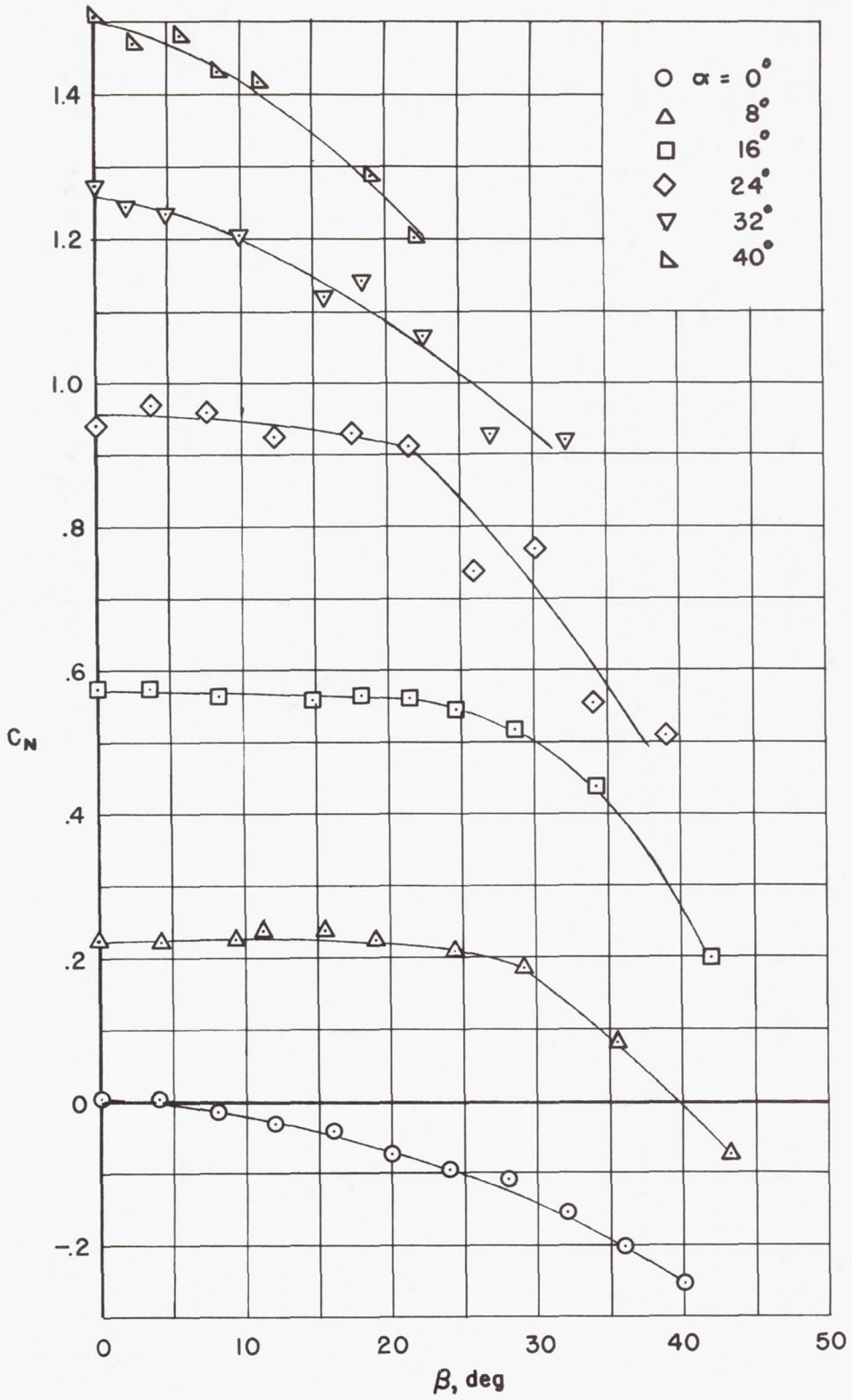
(b) Rolling-moment coefficient versus sideslip angle.

Figure 6.- Continued.



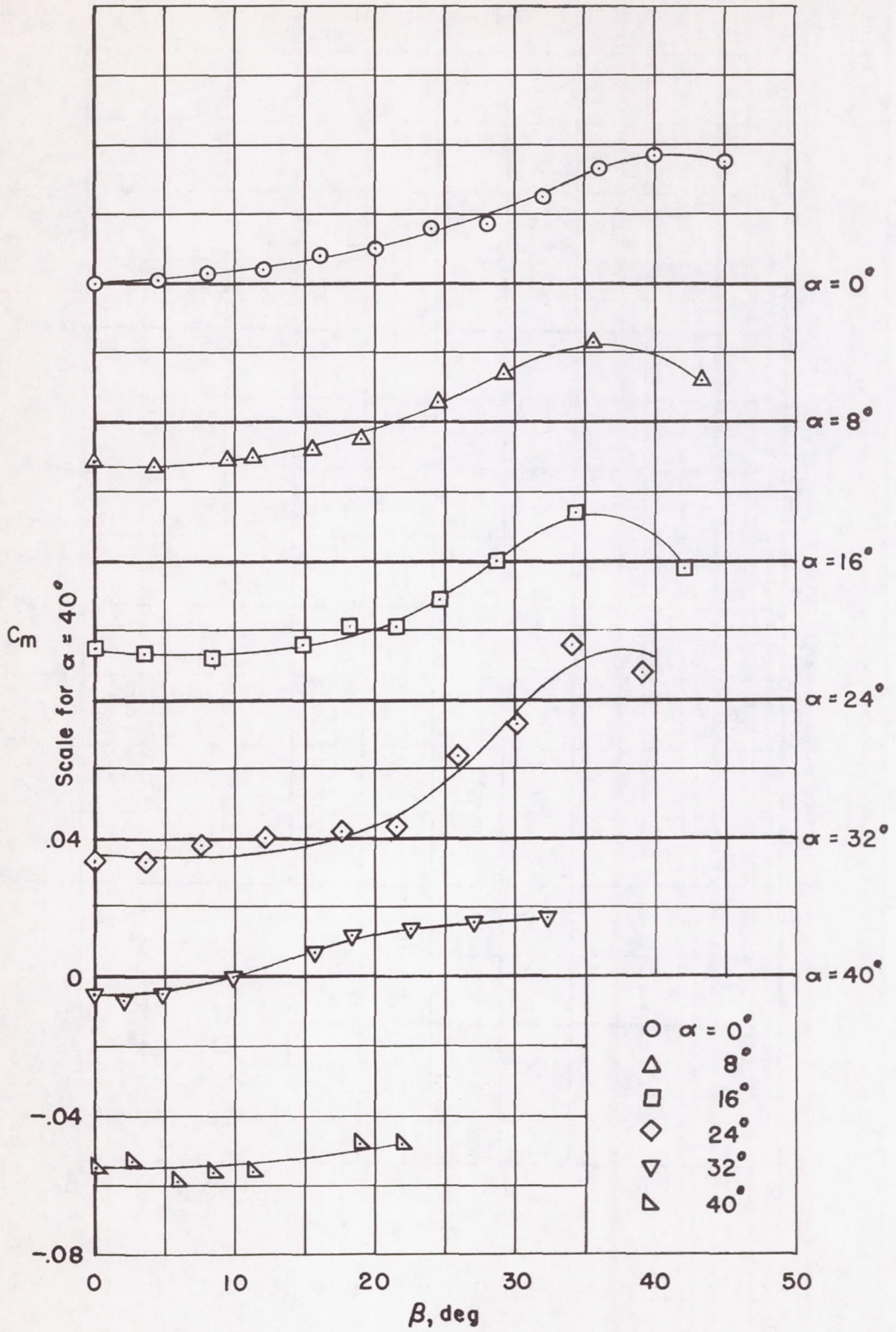
(c) Side-force coefficient versus sideslip angle.

Figure 6.- Continued.



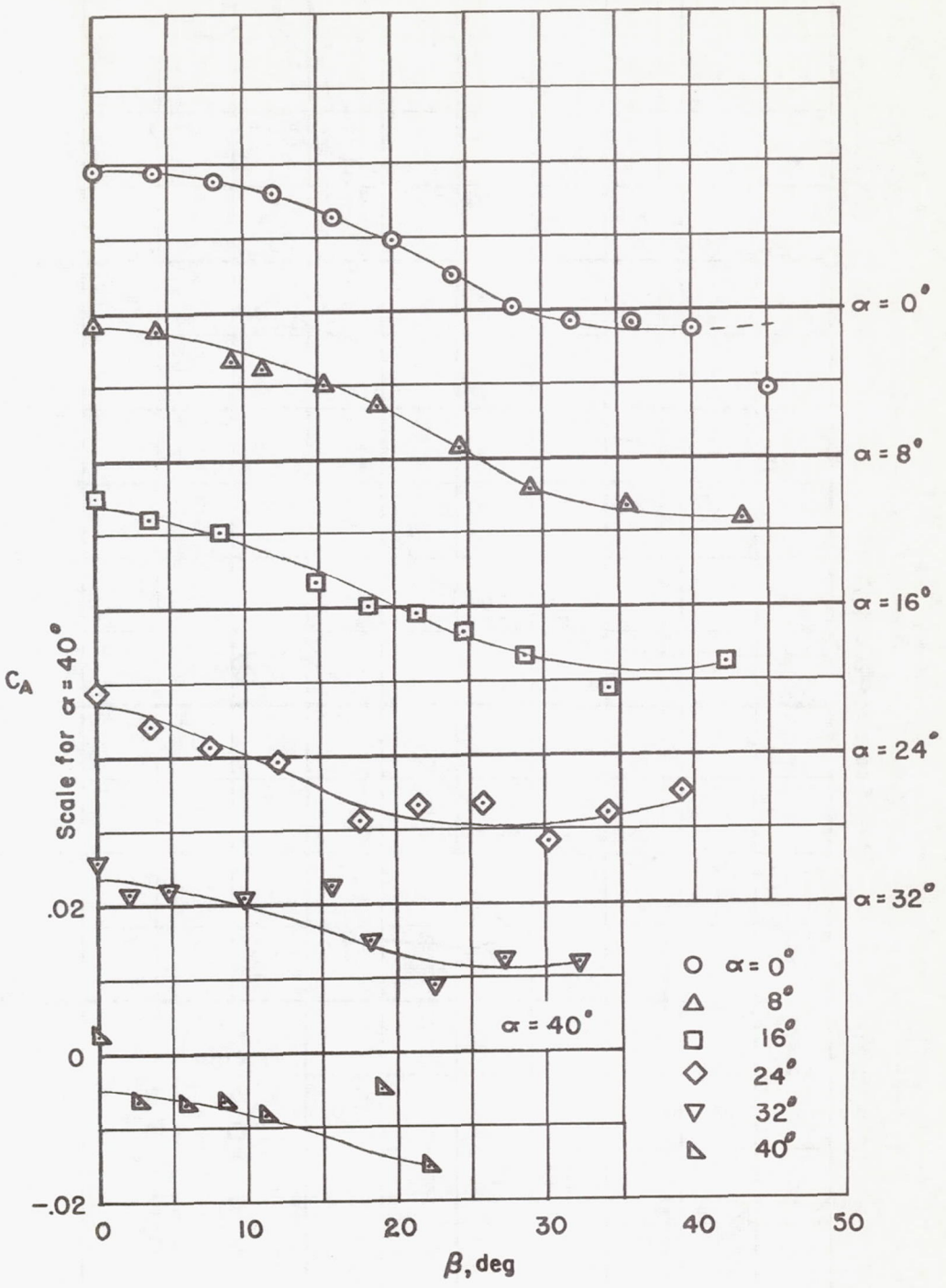
(d) Normal-force coefficient versus sideslip angle.

Figure 6.- Continued.



(e) Pitching-moment coefficient versus sideslip angle.

Figure 6.- Continued.



(f) Axial-force coefficient versus sideslip angle.

Figure 6.- Concluded.

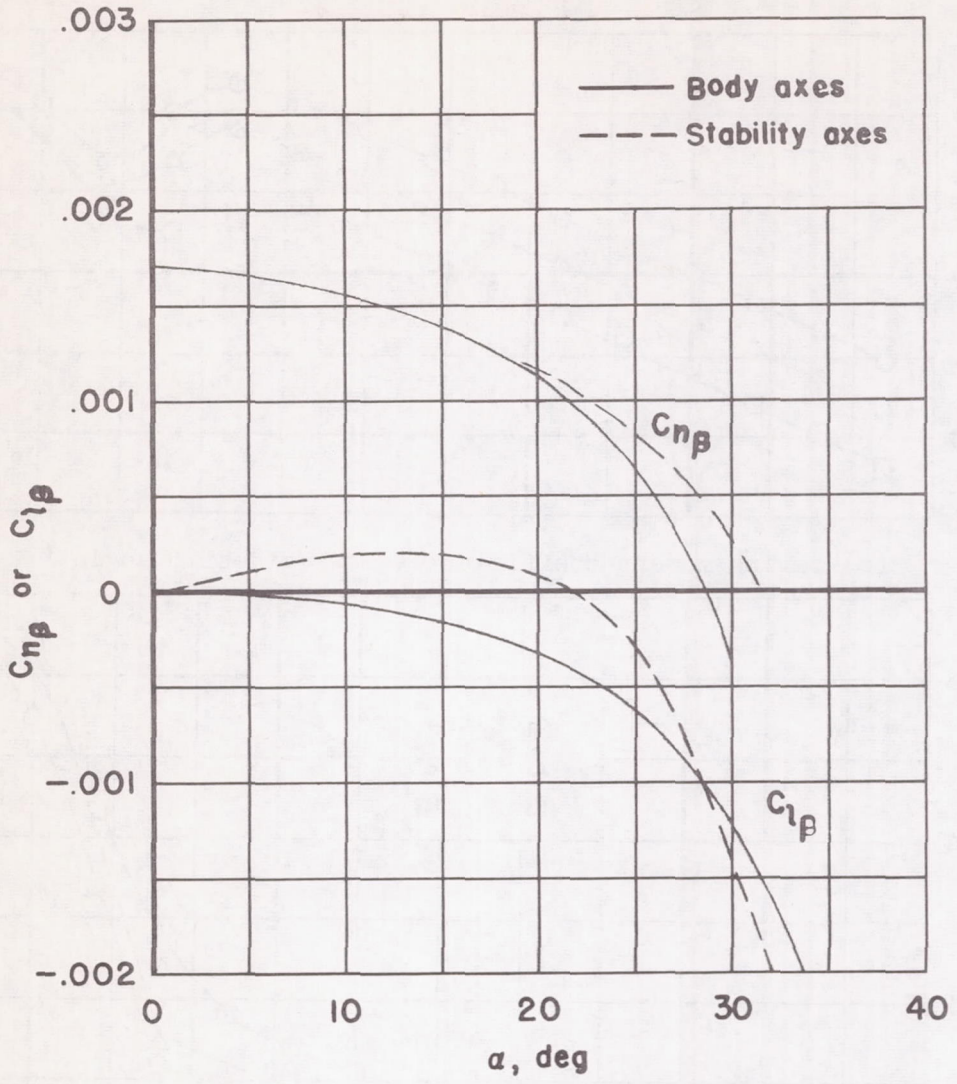
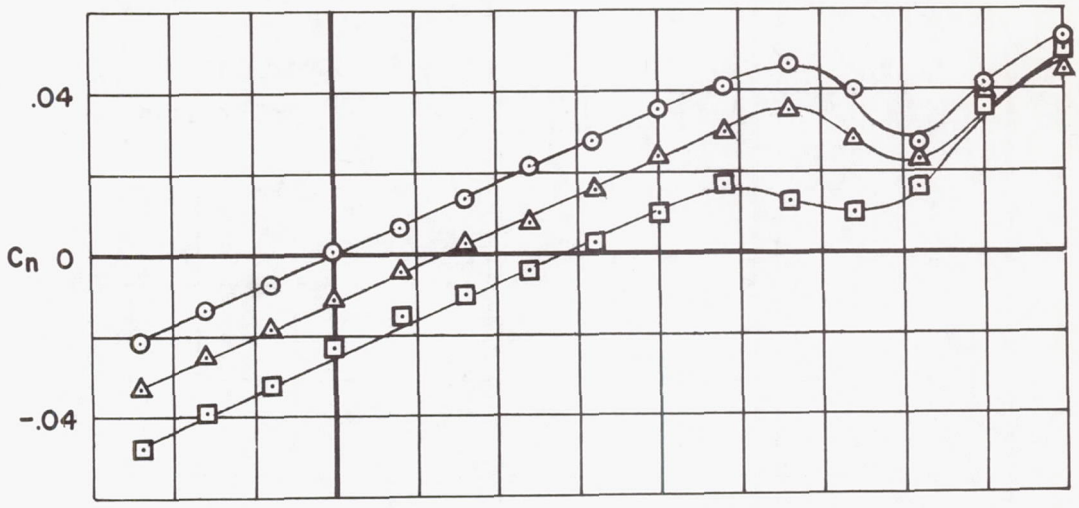
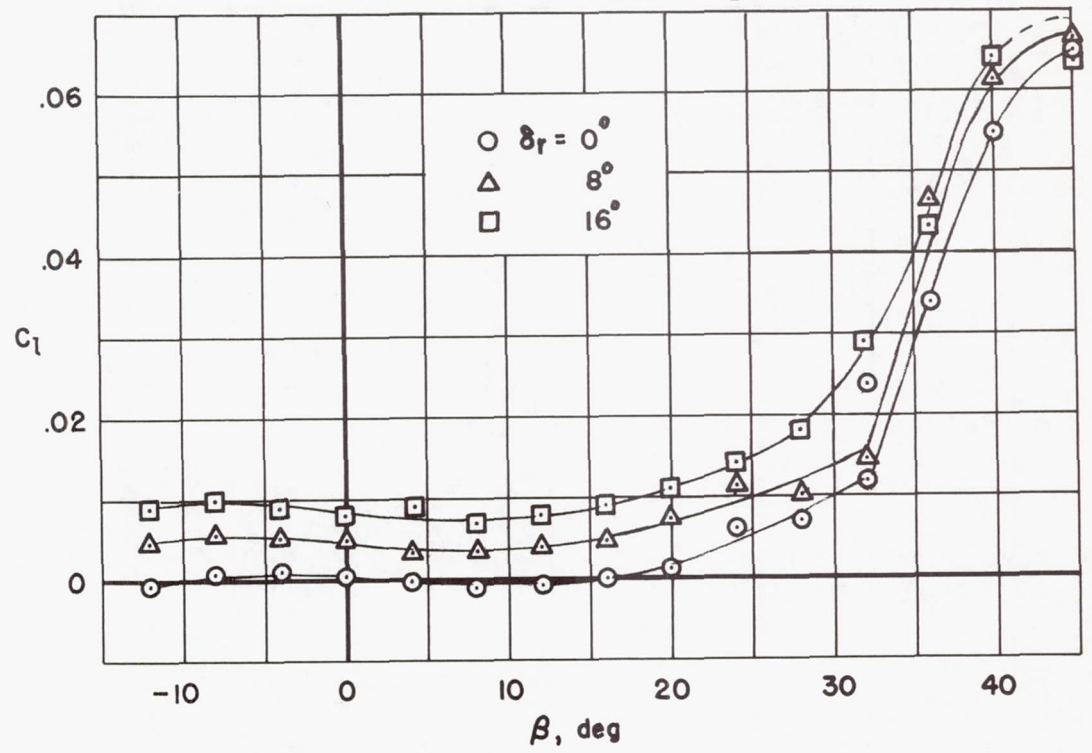


Figure 7.- Variation of C_{l_β} and C_{n_β} with angle of attack; $\Gamma = -30^\circ$.

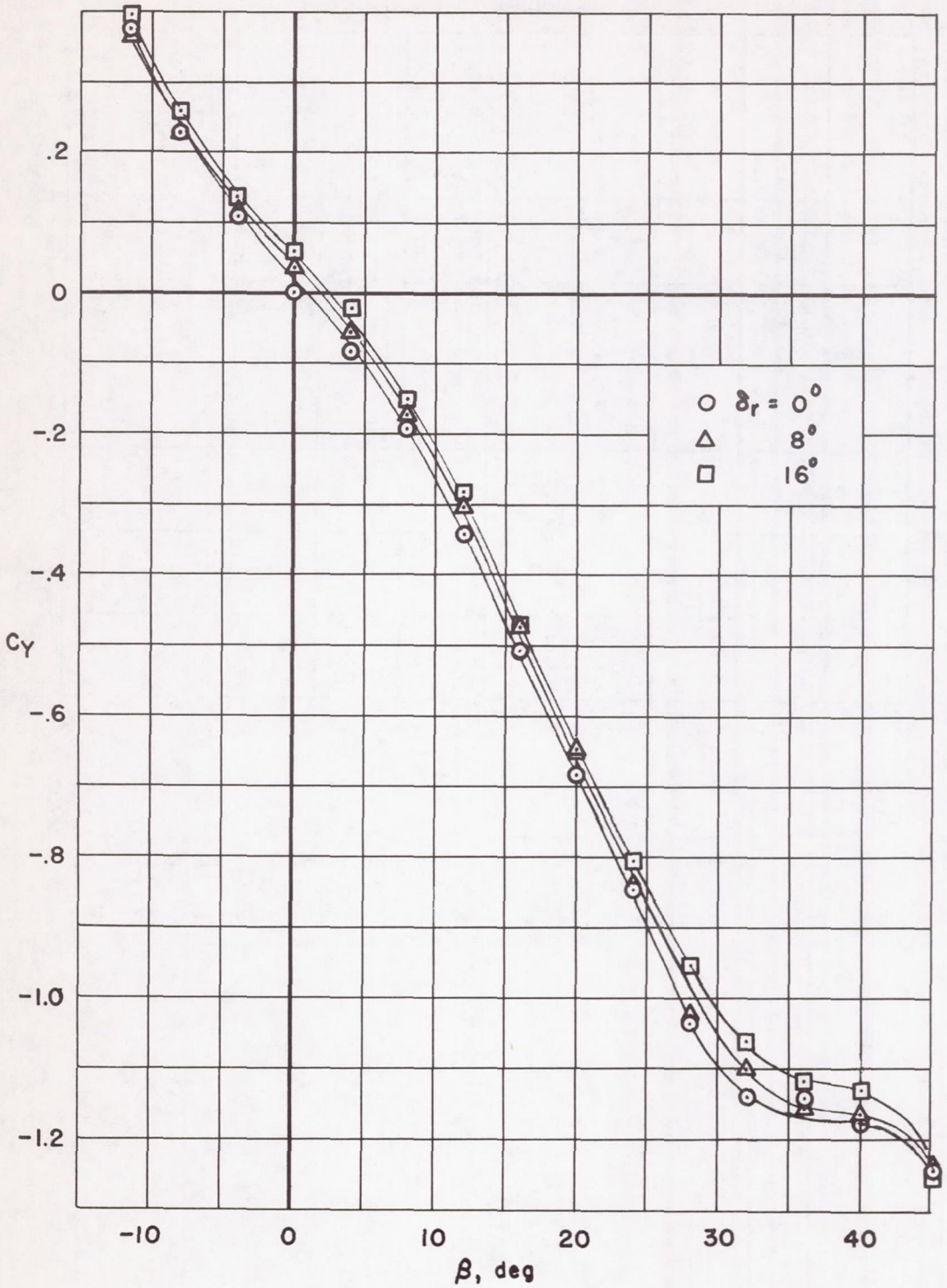


(a) Yawing-moment coefficient versus sideslip angle.



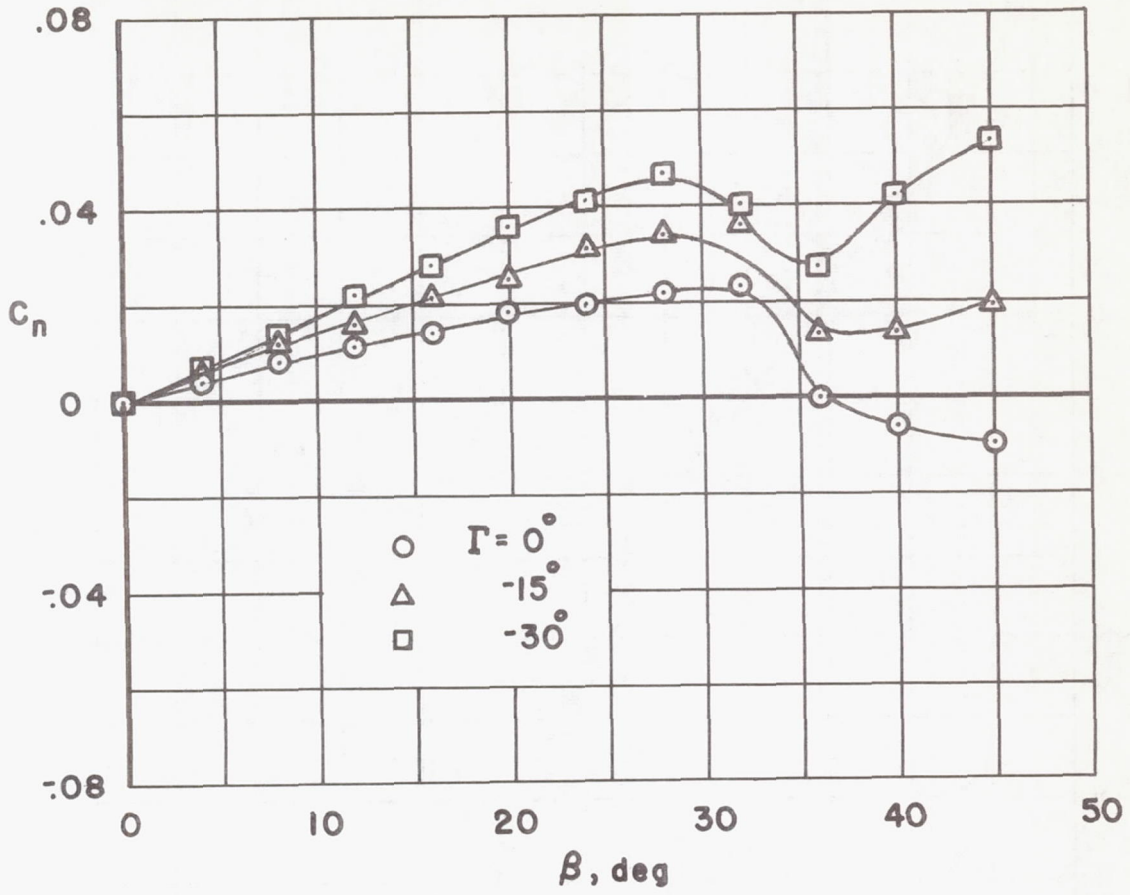
(b) Rolling-moment coefficient versus sideslip angle.

Figure 8.- Static lateral-stability characteristics for several rudder deflections; $\Gamma = -30^\circ$, $\alpha = 0^\circ$.



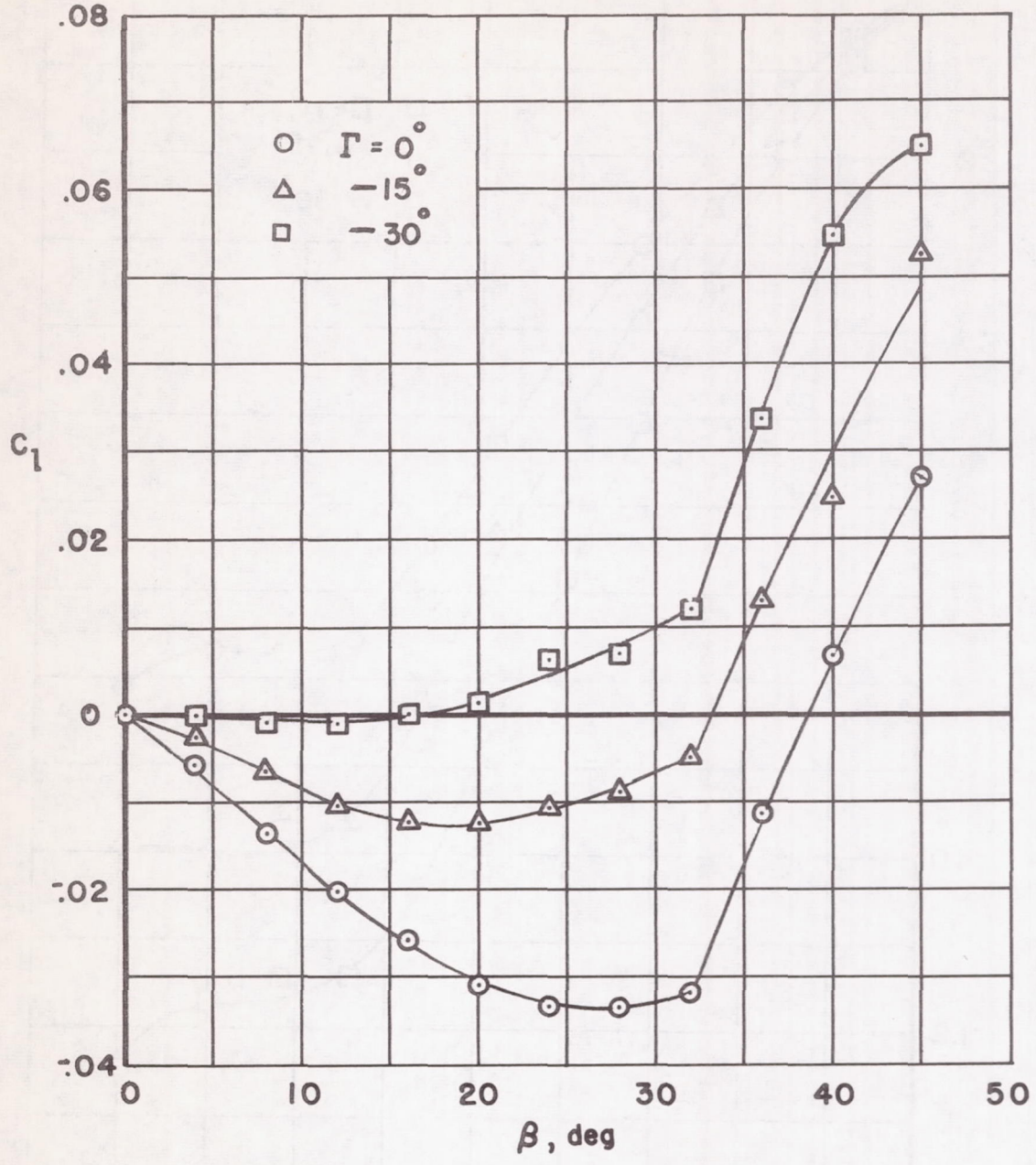
(c) Side-force coefficient versus sideslip angle.

Figure 8.- Concluded.



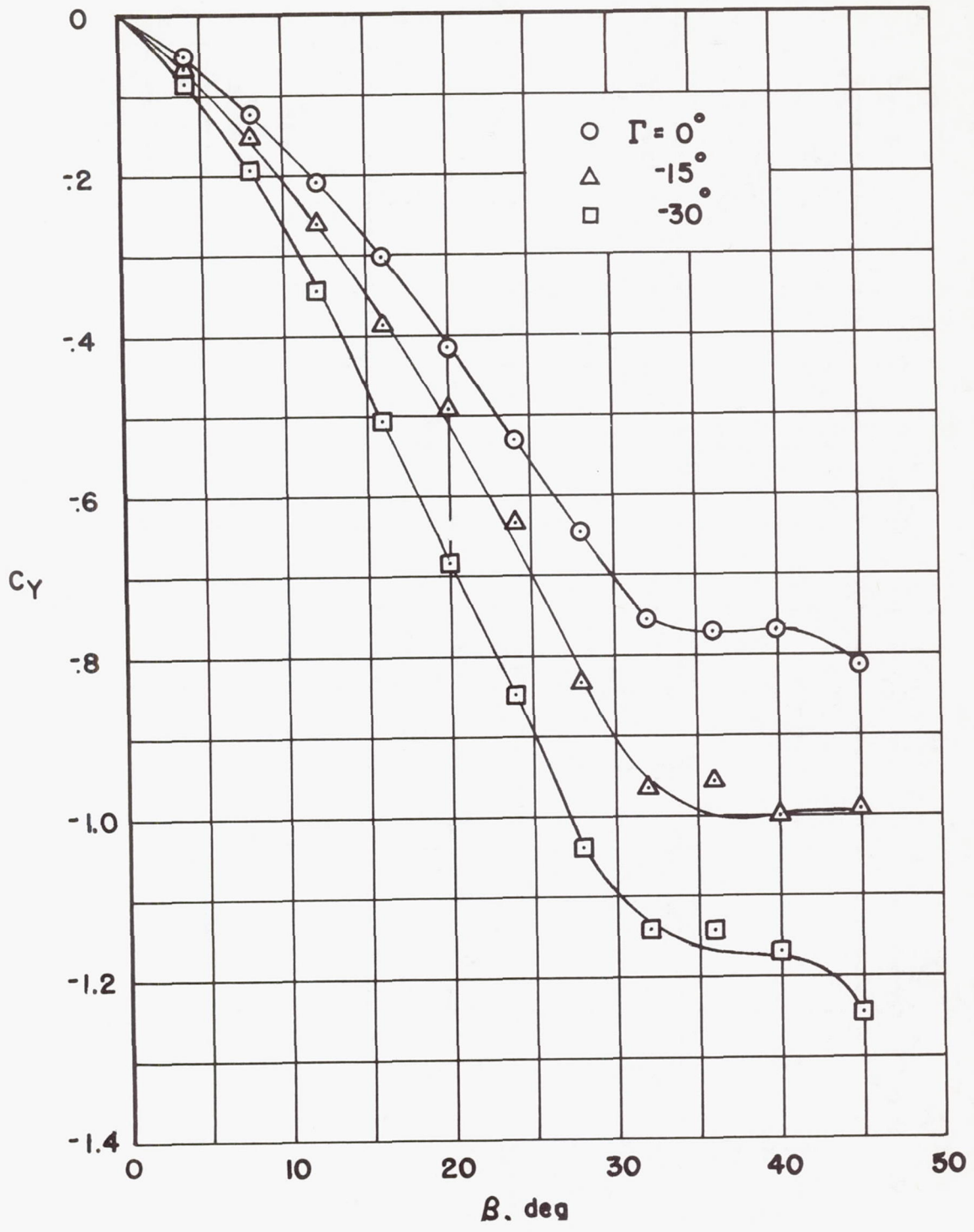
(a) Yawing-moment coefficient versus sideslip angle.

Figure 9.- Static lateral-stability characteristics for several dihedral angles; $\alpha = 0^{\circ}$.



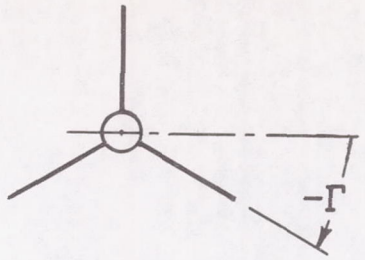
(b) Rolling-moment coefficient versus sideslip angle.

Figure 9.- Continued.



(c) Side-force coefficient versus sideslip angle.

Figure 9.- Concluded.



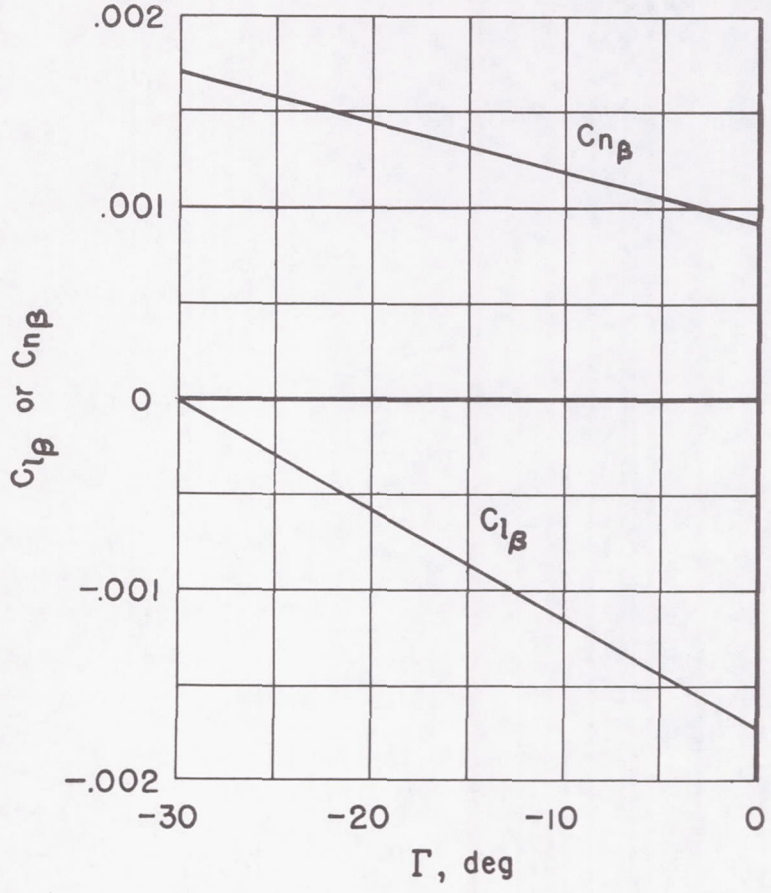


Figure 10.- Variation of C_{l_β} and C_{n_β} with dihedral angle; $\alpha = 0^\circ$.